

Analysis of surface plasmon waves in metal-dielectric-metal structures and the criterion for negative refractive index

Tian Yang and Kenneth B. Crozier

School of Engineering and Applied Sciences, Harvard University, 33 Oxford Street, Maxwell Dworkin, Cambridge, Massachusetts 02138
tianyang@deas.harvard.edu

Abstract: Surface plasmon waves in metal-dielectric-metal structures have been theoretically examined. Because of the existence of evanescent waves that can have comparable or smaller decay rates than the propagating waves, the sign of dispersion does not necessarily indicate the sign of effective refractive index for these structures. By using the direction of energy decay to distinguish the sign of index, we have obtained different results and insights from previous reports. We also propose an approach to increase the bandwidth and decrease the loss of negative index surface plasmon propagation in the MDM structure, by simply changing the properties of its dielectric layer.

©2009 Optical Society of America

OCIS codes: (240.6680) Surface plasmons; (260.2030) Dispersion; (350.3618) Left-handed materials.

References and links

1. V. G. Veselago, "The Electrodynamics of Substances with Simultaneously Negative Values of ϵ and μ ," *Sov. Phys. Usp.* **10**, 509-514 (1968).
2. J. B. Pendry, "Negative Refraction Makes a Perfect Lens," *Phys. Rev. Lett.* **85**, 3966-3969 (2000).
3. D. R. Smith, J. B. Pendry, and M. C. K. Wiltshire, "Metamaterials and Negative Refractive Index," *Science* **305**, 788-792 (2004).
4. Vladimir. M. Shalaev, "Optical negative-index metamaterials," *Nat. Photonics* **1**, 41-48 (2007).
5. C. M. Soukoulis, S. Linden, and M. Wegener, "Negative Refractive Index at Optical Wavelengths," *Science* **315**, 47-49 (2007).
6. Shuang Zhang, Wenjun Fan, N. C. Panoiu, K. J. Malloy, R. M. Osgood, and S. R. J. Brueck, "Experimental Demonstration of Near-Infrared Negative-Index Metamaterials," *Phys. Rev. Lett.* **95**, 137404 (2005).
7. V. M. Shalaev, W. Cai, U. K. Chettiar, H.-K. Yuan, A. K. Sarychev, V. P. Drachev, and A. V. Kildishev, "Negative index of refraction in optical metamaterials," *Opt. Lett.* **30**, 3356-3358 (2005).
8. G. Dolling, C. Enkrich, M. Wegener, C. M. Soukoulis, and S. Linden, "Simultaneous Negative Phase and Group Velocity of Light in a Metamaterial," *Science* **312**, 892-894 (2006).
9. G. Dolling, M. Wegener, C. M. Soukoulis, and S. Linden, "Negative-index metamaterial at 780 nm wavelength," *Opt. Lett.* **32**, 53-55 (2007).
10. G. Dolling, M. Wegener, and S. Linden, "Realization of a three-functional-layer negative-index photonic metamaterial," *Opt. Lett.* **32**, 551-553 (2007).
11. J. Valentine, S. Zhang, T. Zentgraf, E. Ulin-Avila, D. A. Genov, G. Bartal, and X. Zhang, "Three Dimensional Optical Metamaterial Exhibiting Negative Refractive Index," *Nature* **455**, 376-379 (2008).
12. D. R. Smith, D. Schurig, M. Rosenbluth, S. Schultz, S. A. Ramakrishna, and J. B. Pendry, "Limitations on subdiffraction imaging with a negative refractive index slab," *Appl. Phys. Lett.* **82**, 1506-1508 (2003).
13. H. Shin and S. Fan, "All-Angle Negative Refraction for Surface Plasmon Waves Using a Metal-Dielectric-Metal Structure," *Phys. Rev. Lett.* **96**, 073907 (2006).
14. E. N. Economou, "Surface Plasmons in Thin Films," *Phys. Rev.* **182**, 539 (1969).
15. H. J. Lezec, J. A. Dionne, and H. A. Atwater, "Negative Refraction at Visible Frequencies," *Science* **316**, 430-432 (2007).
16. Eyal Feigenbaum, Noam Kaminski, and Meir Orenstein, "Negative Group Velocity: Is It a Negative Index Material or Fast Light?" in *Tech. Dig. OSA Topical Meeting - Slow and Fast Light*, (Boston, MA, 2008), SWB4; [arXiv:0807.4915v1](https://arxiv.org/abs/0807.4915v1) [physics.optics].
17. A. D. Rakic, A. B. Djuricic, J. M. Elazar, and M. L. Majewski, "Optical properties of metallic films for vertical-cavity optoelectronic devices," *Appl. Opt.* **37**, 5271-5283 (1998).

18. S. A. Maier, *Plasmonics: Fundamentals and Applications*, Ch 2 (Springer, 2007).
19. P. Tournois and V. Laude, "Negative group velocities in metal-film optical waveguides," *Opt. Commun.* **137**, 41-45 (1997).
20. G. Shvets, "Photonic approach to making a material with a negative index of refraction," *Phys. Rev. B* **67**, 035109 (2003).
21. J. A. Dionne, L. A. Sweatlock, H. A. Atwater, and A. Polman, "Plasmon slot waveguides: Towards chip-scale propagation with subwavelength-scale localization," *Phys. Rev. B* **73**, 035407 (2006).
22. Consider a lossless material. Since energy is conserved, a wave packet must not evanescently decay as it propagates. Therefore, a group of evanescent waves, each corresponding to a different (ω, β) pair, can not form a propagating wave packet.
23. M. Nezhad, K. Tetz, and Y. Fainman, "Gain assisted propagation of surface plasmon polaritons on planar metallic waveguides," *Opt. Express* **12**, 4072-4079 (2004).
24. A. K. Popov and V. M. Shalaev, "Compensating losses in negative-index metamaterials by optical parametric amplification," *Opt. Lett.* **31**, 2169-2171 (2006)
25. A. K. Popov and V. M. Shalaev, "Negative-index metamaterials: second-harmonic generation, Manley-Rowe relations and parametric amplification," *Appl. Phys. B* **84**, 131-137 (2006).
26. M. I. Stockman, "Criterion for Negative Refraction with Low Optical Losses from a Fundamental Principle of Causality," *Phys. Rev. Lett.* **98**, 177404 (2007).
27. N. M. Litchinitser, I. R. Gabitov, A. I. Maimistov, and V. M. Shalaev, "Negative refractive index metamaterials in optics," Emil Wolf Ed., *Progress in Optics*, vol. 51, Ch 1 (Elsevier, 2008).
28. J. A. Dionne, E. Verhagen, A. Polman, and H. A. Atwater, "Are negative index materials achievable with surface plasmon waveguides? A case study of three plasmonic geometries," *Opt. Express* **16**, 19001-19017 (2008).

1. Introduction

Negative index material (NIM) is a particularly interesting example of artificially engineered metamaterial, whose refractive index has a negative real part [1-3]. When an electromagnetic wave propagates inside a NIM, its energy and wave fronts propagate in opposite directions. Negative refraction of the propagating waves and amplification of the evanescent waves at the boundary between a positive index material and a NIM have been proposed for sub-wavelength imaging [2].

NIMs were first implemented by assemblies of resonant elements on a deep subwavelength scale, which are difficult to fabricate for applications at optical frequencies [4-12]. In 2006, Shin and Fan theoretically proposed an all-angle negative refraction lens at optical frequencies, which does not rely on resonant components and is flat at an atomic level [13]. The proposed NIM consists of metal-dielectric-metal (MDM) layers, a planar structure that was studied as early as 1969 [14]. Later, Lezec *et al.* reported experimental observation of negative refraction inside a MDM structure in the visible frequency range [15]. Recently, Feigenbaum *et al.* suggested that fast light could be responsible for the negative refraction observed by Lezec *et al.* [16] Because of the high ohmic loss rates from metals in this structure, care must be taken to distinguish between propagation and evanescence when studying the behaviors of waves. In our paper, we will present a careful examination of the solutions to the equations of surface plasmon waves in the MDM structure. Our results will identify the existence of a variety of propagating and evanescent surface plasmon waves. The evanescent decay rates of the latter can be comparable to, or smaller than, the ohmic loss rates of the former. Consequently, the criterion of dispersion and phase velocity having opposite signs does not necessarily indicate negative index, which is only applicable to propagating waves. By using the direction of energy decay as the criterion for identifying the sign of index, we have obtained different conclusions from previous reports.

2. Surface plasmon waves in metal-dielectric-metal structure

Let's solve for the surface plasmon modes of the 2-D MDM structure in Fig. 1, in which a thin layer of silicon nitride is sandwiched between gold half-spaces. In our calculation, we have used the experimentally-measured values for relative permittivity ϵ/ϵ_0 of gold at different frequencies, ϵ_{Au} , reported in Ref. 17. The relative permittivity ϵ/ϵ_0 of silicon nitride, ϵ_{SN} , is set to 4. Surface plasmons in this structure are TM polarized, i.e., the magnetic field has only a y-polarized component. We will only consider TM polarization in this paper. By satisfying

boundary conditions at metal-dielectric interfaces and letting the fields decay to zero at $z = \pm\infty$, the dispersion relations of the TM polarized modes can easily be obtained as below [18].

$$e^{-k_{SN}d} \mp \frac{k_{SN} / \epsilon_{SN} + k_{Au} / \epsilon_{Au}}{k_{SN} / \epsilon_{SN} - k_{Au} / \epsilon_{Au}} = 0 \quad (1)$$

$$k_{SN,Au} = (\beta^2 - k_0^2 \epsilon_{SN,Au})^{1/2} \quad (2)$$

In Eq. (1), “-” is for antisymmetric modes, and “+” is for symmetric modes. When we discuss symmetry in this paper, we are referring to the symmetry of electric fields with respect to the center plane of the dielectric layer in the MDM structure. The field profile in the upper gold half-space follows $\exp(-k_{Au}z)\exp(i\beta x)$. Similarly, the field profile in the lower gold half-space follows $\exp(k_{Au}z)\exp(i\beta x)$. In the dielectric region, the field profile follows $A \exp(k_{SN}z)\exp(i\beta x) + B \exp(-k_{SN}z)\exp(i\beta x)$, where A and B are constants. $k_0 = \omega/c$ is the wave vector in vacuum, and $d=40 \text{ nm}$ is the thickness of the dielectric layer. We define the square root in Eq. (2) such that $\text{Real}(k) \geq 0$. Let $\beta = \beta' + i\beta''$, where β' and β'' represent the real and imaginary parts of β , respectively. In this paper, we define β' to be non-negative, meaning that the phase front always propagates along the $+x$ direction, as the time dependence is taken as $e^{-i\omega t}$. A positive or negative β'' value signifies exponential decay of energy along the $+x$ or $-x$ direction, respectively. The dispersion relations are calculated by finding the zeros of Eq. (1) at each frequency.

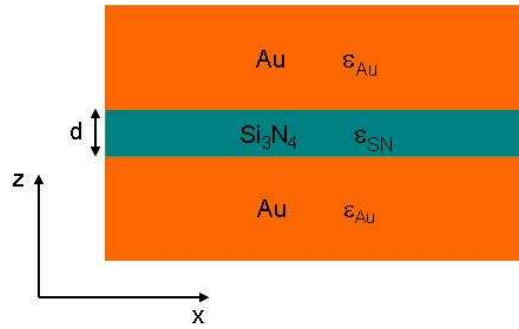


Fig. 1. A planar metal-dielectric-metal structure. $d = 40 \text{ nm}$ is used unless otherwise stated.

First we will consider a hypothetical situation for which there is no ohmic loss. The imaginary part of ϵ_{Au} is set to 0, while the real part is kept, again taken from Ref. 17. This violates the Kramers-Kronig relations but is appropriate for our purpose of identifying the surface plasmon modes. Figure 2 shows the calculated dispersion relations of the antisymmetric and symmetric modes. In each of Fig. 2(a) and 2(b), the values of β' and β'' at each frequency for a set of modes are plotted as red and blue curves, respectively. Similarly, green and yellow curves are used for the values of β' and β'' , respectively, for other modes. It should be noted that two pairs of colors are used purely to make the diagrams clearer and have no other meanings. In a lossless structure, there is no energy decay as a wave propagates, therefore $\beta''=0$ for propagating modes, while the curves with $\beta'' \neq 0$ correspond to the evanescent modes.

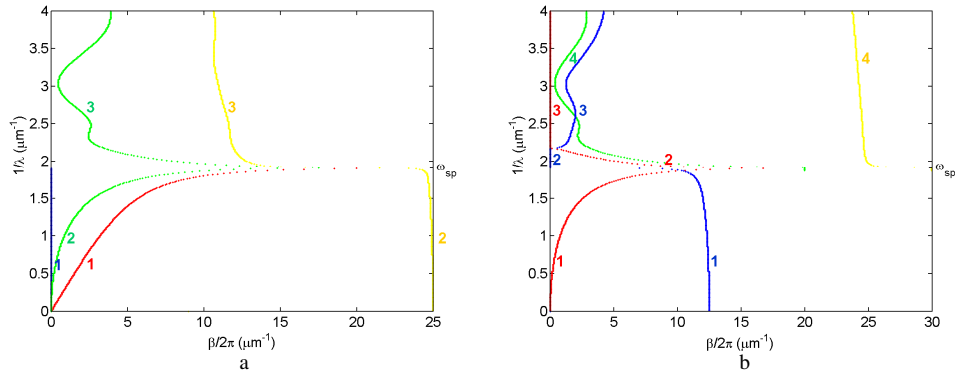


Fig. 2. Dispersion diagrams for a planar structure consisting of a 40 nm thick silicon nitride layer sandwiched between lossless gold half-spaces. Red and blue curves correspond to the real and imaginary parts, respectively, of $\beta/2\pi$ at each frequency $1/\lambda$ for some modes. λ is free space wavelength. Similarly, the green and yellow curves correspond to the real and imaginary parts for other modes. (a) Antisymmetric modes. (b) Symmetric modes.

There are several important features to be noticed in Fig. 2: There is one antisymmetric propagating mode below ω_{sp} [18], labeled '1', and one symmetric propagating mode immediately above ω_{sp} , labeled '2'. ω_{sp} is the asymptotic value of surface plasmon frequency at a lossless metal-dielectric interface when the surface plasmon wavelength approaches zero. The symmetric propagating mode has negative group velocity values and has been proposed by Shin and Fan as a means for obtaining negative refractive index and sub-wavelength imaging [13, 18-20]. When the dielectric layer is thicker than a critical thickness, the frequency of the symmetric propagating mode at $\beta = 0$ drops below ω_{sp} , and its refractive index becomes positive. There are an infinite number of higher order evanescent modes with larger β'' values which have not been plotted. In the dispersion diagrams, the distances between the β'' curves of different order evanescent modes decrease with increase in the dielectric layer thickness. When the dielectric layer is thicker than a cutoff thickness, metal clad waveguide modes will show up, which have not been plotted either [21].

For propagating waves, if the group velocity $v_g = d\omega/d\beta'$ and the phase velocity $v_p = \omega/\beta'$ have opposite signs, the material exhibits negative refractive index. However, for evanescent waves, no wave packet can be formed by summing up a group of monochromatic waves, each corresponding to a different $(\omega, \beta' + i\beta'')$ point in the dispersion diagram [22]. Therefore group velocity loses its physical meaning when evanescent waves are being considered, and the sign of the dispersion quantity $d\omega/d\beta'$ can not be used to determine the sign of refraction. This normally does not present problems for studying low loss materials, because the evanescent waves decay much faster than the propagating waves and it is easy to distinguish between the two. However, surface plasmons at optical frequencies suffer from high ohmic loss rates, which can be high enough to be comparable to the evanescent decay rates for the case of MDM structures. In the following, we will identify the propagating and evanescent waves in the lossy structure by comparing it to the lossless case. We will determine the sign of refractive index for both propagating waves and evanescent waves from the direction of energy velocity v_e . In a lossy material having no variation along the direction of v_e , v_e is in the same direction as the decay rate of energy amplitude β'' , and β'' and n have the same sign. For propagating waves, β'' corresponds to dissipation of electromagnetic power. For evanescent waves, β'' corresponds to the sum of both evanescent decay and power dissipation. When the evanescent decay rates are comparable to or lower than the propagation loss rates, the evanescent waves could contribute in various refraction experiments as well. Note that, in a lossless material, $v_e \beta'' = 0$. In order to relate the direction of energy propagation to the sign of β'' , loss must be included.

In order to identify the surface plasmon modes in a lossy structure with the modes in the lossless case, note that under the lossless condition, the time reverse of a solution to the Maxwell equations is also a solution. Therefore, for each point in the dispersion diagram of Fig. 2, there is a corresponding point with the same β' value but with β'' having the same magnitude but opposite sign. So in Fig. 2 we have plotted only half of the dispersion diagram. An important concept is that an evanescent mode with $\beta' \neq 0$ is not the same mode as its time reverse – although the magnitudes of β'' are the same. When loss is included, such a pair of modes would correspond to two dispersion points with different magnitudes of β'' . The difference between two such modes is explained in Fig. 3. Because $\beta' \neq 0$, there will be power flowing along the x -direction in both dielectric and metal, but in opposite directions so that there is zero total power flow along the x -direction for the evanescent modes under the lossless condition. If the power flows in the $+x$ direction in the dielectric and in the $-x$ direction in the metal, as in Fig. 3(a), there must be net power leaving the dielectric for the metal in order to have the energy density decay in the $+x$ direction. The power flow in the dielectric decays by being converted to flow in the backward direction in the metal. Its time reverse, illustrated in Fig. 3(b), is a different mode which has net power leaving the metal for the dielectric. When loss is included, there will be non-zero total power going in the direction of decay, in order to provide energy for ohmic heating. The modes in Fig. 3(a) and 3(b) will then contain more power in the dielectric and the metal, respectively. Through dispersion calculations, it will be shown that each point on the dispersion diagram of the lossless structure, illustrated in Fig. 2, that corresponds to a evanescent mode and has $\beta' \neq 0$, corresponds to one positive index mode and one negative index mode of the lossy structure. The other points on the dispersion diagram of the lossless structure correspond to only one mode each of the lossy structure, because each of them is essentially the same mode as its time reverse: for lossless propagating modes, there is zero net power conversion between the dielectric and the metal; for lossless bandgap modes with $\beta' = 0$, there is no power flowing along the x - direction inside the dielectric or the metal.

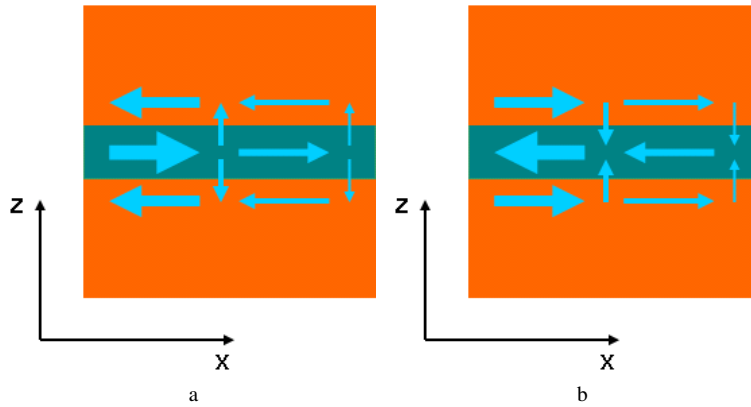


Fig. 3. Schematic mode profiles of a pair of evanescent modes with $\beta' \neq 0$, which are time-reverse to each other under the lossless condition. The arrows indicate the directions and magnitudes of power flows, which have been integrated within each layer.

Figure 4 presents dispersion diagrams of the lossy structure, in which the imaginary part of ϵ_{Au} has been included in the calculation. Let us identify the lossy surface plasmon modes in Fig. 4 with the lossless modes in Fig. 2. With loss, the signs of n and v_e can be determined from, and are the same as, the sign of β'' . The red/blue and green/yellow curves show the values of β' and β'' for different modes. First let us compare the dispersion diagrams of antisymmetric modes in Fig. 2(a) and 4(a). There is one dispersion curve below ω_{sp} in Fig. 2(a), and below a similar turning frequency in Fig. 4(a), that corresponds to a propagating

mode, as shown by the red and blue curves labeled ‘1’. The evanescent modes above ω_{sp} in Fig. 2(a), labeled ‘3’, split into two very different sets of dispersion curves in Fig. 4(a), labeled ‘3a’ and ‘3b’, the ‘a’ modes having β'' , $n > 0$ and much smaller decay rates than the ‘b’ modes which has β'' , $n < 0$. The evanescent mode below ω_{sp} in Fig. 2(a) also split into two set of curves in Fig. 4(a), labeled ‘2’, but only the one with $n < 0$ is plotted. Part of the red curve in Fig. 4(a), labeled ‘f’, shows negative dispersion around $1/\lambda \sim 2 \mu\text{m}^{-1}$, i.e. a free space wavelength λ of 500 nm. Although the corresponding decay rates are small, this negative dispersion regime clearly corresponds to evanescent behavior because v_e and $d\omega/d\beta$ have opposite signs. Therefore this negative dispersion but positive index regime of the lossy structure corresponds to the lossless evanescent part above ω_{sp} in Fig. 2(a), labeled ‘3’, instead of corresponding to part of the lossless propagating mode, labeled ‘1’. Next let us compare the symmetric modes under lossless and lossy conditions, as shown in Fig. 2(b) and 4(b). The lossless evanescent mode below ω_{sp} in Fig. 2(b), labeled ‘1’, split into two dispersion curves in Fig. 4(b), labeled ‘1a’ and ‘1b’, one with $n > 0$ and the other with $n < 0$. The lossless evanescent modes a distance above ω_{sp} and with $\beta' = 0$, labeled ‘3’ in Fig. 2(b), correspond to just one dispersion curve with $n > 0$ in the lossy structure, labeled ‘3’ in Fig. 4(b). The negative index propagating mode right above ω_{sp} in Fig. 2(b), and right above a similar turning frequency in Fig. 4(b), both labeled ‘2’, exhibit negative dispersion and negative v_g as shown by the red curves, and zero or negative β'' values, as shown by the blue curves. The curves labeled ‘4’ in Fig. 2(b) and 4(b) correspond to evanescent modes with higher decay rates.

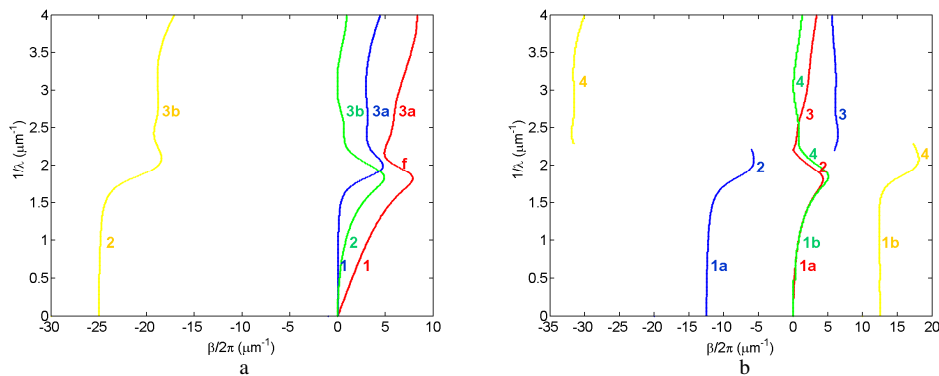


Fig. 4. Dispersion diagrams for a planar structure consisting of a 40 nm thick silicon nitride layer sandwiched between gold half-spaces, ohmic loss included. Red and blue curves correspond to the real and imaginary parts, respectively, of $\beta/2\pi$ at each frequency $1/\lambda$ for some modes. λ is free space wavelength. Similarly, the green and yellow curves correspond to the real and imaginary parts for other modes. (a) Antisymmetric modes. (b) Symmetric modes.

3. Discussion on negative index behavior

Having identified the surface plasmon waves in the MDM structure by categorizing them into antisymmetric/symmetric and propagating/evanescent modes, let us discuss application of this structure as a negative index material. In Fig. 4, the antisymmetric mode labeled ‘f’ and the symmetric mode labeled ‘2’ both demonstrate negative dispersion and relatively low decay rates, are both in a similar frequency range, but correspond to opposite signs of refractive indices. Often different metals are used for the upper and lower metals in the MDM structure, which makes it impossible to differentiate the modes by symmetry [13, 15]. In such situations, if we plot a complete dispersion diagram, the positive index evanescent modes, ‘f’, and the negative index propagating modes, ‘2’, will appear together at similar frequencies, both showing negative dispersion and being capable to transport energy at similar decay rates. This

observation tell us that, in such a structure having high ohmic losses, propagating and evanescent modes may not be distinguished from each other by the amplitudes of decay rates, and the sign of dispersion can not be simply applied to determine the sign of refraction. Which type of mode will be more dominantly excited is dependent on the experiment design and conditions [13, 15]. As a rule of thumb, more power being excited inside the metal corresponds to negative refractive index, and vice versa [16, 19]. From this discussion, we believe the negative refraction of MDM experimentally observed by Lezec *et. al* is indicative of negative index [15].

Gain media have been proposed to compensate ohmic loss for propagating modes [23-25]. Gain will affect evanescence behavior in a different manner. Comparing Fig. 2(a) and 4(a), the decay rates of the positive index evanescent modes, labeled '3', '3a' and 'f', are even larger when ohmic loss is ignored. Using a theory similar to the Kramers-Kronig relations, Stockman predicted that, in order to have negative index behavior, loss should not be compensated too much [26].

The ultimate goals of NIM design include a large negative $Real(n)$, a large Figure of Merit $FOM = |Real(n)/Imag(n)|$, a broad bandwidth and optimized impedance matching [27]. The bandwidth of negative index behavior of MDM structures can be increased by thinning the dielectric layer, while employing a higher index dielectric material to obtain the same center frequency [28]. Fig. 5 shows the calculated dispersion diagram of propagating modes in a 20 nm thick silicon layer sandwiched by gold half-spaces. The refractive index of silicon is taken as 4. Optical absorption in crystalline silicon is much weaker than in gold at visible frequencies, and is ignored in the calculation. Comparing Fig. 5 with the '2' mode in Fig. 4(b) reveals that the NIM band is extended from the blue and green frequency range to almost the entire visible frequency range. The loss of the NIM is also reduced.

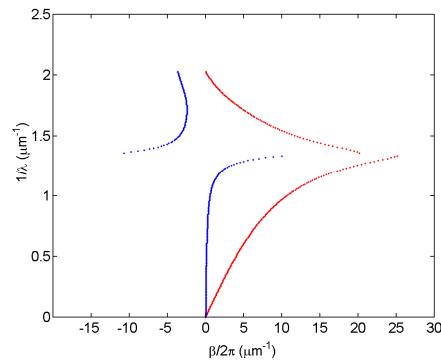


Fig. 5. Dispersion relations for a planar structure consisting of a 20 nm thick silicon layer sandwiched between gold half-spaces. Red and blue curves correspond to the real and imaginary parts of $\beta/2\pi$ at each inverse wavelength $1/\lambda$. λ is free space wavelength.

4. Summary

We have studied the surface plasmon waves in the MDM structure by solving dispersion equations and comparing solutions under lossless and lossy conditions. The surface plasmon waves are categorized into antisymmetric/symmetric and propagating/evanescent modes. The sign of refractive index has been determined by the direction of energy decay, for both propagating and evanescent waves. It has been found that, because of ohmic loss in the MDM structure, some evanescent modes can transport energy at similar or lower decay rates than the propagating modes, which makes it inappropriate to judge the sign of refractive index from the sign of dispersion. Also shown is that a thinner dielectric layer in the MDM structure leads to a larger bandwidth and a lower loss of the negative index symmetric propagating mode. We believe that, by clarifying the properties of surface plasmon waves in the MDM structure, our

study will facilitate future theoretical and experimental work on metamaterials containing multiple metal-dielectric interfaces.

Acknowledgments

This work was supported by the Microsystems Technology Office (MTO) of the Defense Advanced Projects Agency (DARPA) and the Charles Stark Draper Laboratory.